Journal of Nuclear Materials 407 (2010) 78–82

Contents lists available at ScienceDirect

Journal of Nuclear Materials

journal homepage: www.elsevier.com/locate/jnucmat

High temperature fracture characteristics of a nanostructured ferritic alloy (NFA)

Thak Sang Byun *, Jeoung Han Kim [1], Ji Hyun Yoon [1], David T. Hoelzer

Oak Ridge National Laboratory, Oak Ridge, TN 37831, USA

ARTICLE INFO

Article history:
Received 17 July 2010
Accepted 21 September 2010

ABSTRACT

The nanostructured ferritic alloys (NFAs) have been developed to improve high temperature strength and radiation resistance by refining grains and including nanoclusters. Among the key properties of NFAs needed to be assessed for advanced reactor applications the cracking resistance at high temperatures has not been well known. In this work, therefore, the high temperature fracture behavior has been investigated for the latest nanostructured ferritic alloy 14YWT (SM10). The fracture toughness of the alloy was above 140 MPa $\sqrt{m}$ at low temperatures, room temperature (RT) and 200 °C, but decreased to a low fracture toughness range of 52–82 MPa $\sqrt{m}$ at higher temperatures up to 700 °C. This behavior was explained by the fractography results indicating that the unique nanostructure of 14YWT alloy produced shallow plasticity layers at high temperatures and a low-ductility grain boundary debonding occurred at 700 °C. The discussion also proposes methods to improve resistance to cracking.

Published by Elsevier B.V.

1. Introduction

The nanostructured ferritic alloys (NFAs) are mechanically-alloyed composite materials of fine-grained ferritic steel matrix and Y–Ti–O–Fe enriched nanoclusters [1–11]. One of the latest NFAs under development is the 14%Cr steel-based 14YWT produced at Oak Ridge National Laboratory (ORNL) [1,2,10–13]. This alloy is strengthened by grain refinement to a few hundred nanometers and by dispersion of high density nanoclusters. In the past several years this alloy has been considered as the most promising candidate for an advanced reactor core material because of its high temperature strength and high resistance to radiation-induced degradation [3–8,13–18]. Currently, the 14YWT alloy is still being improved and newer heats are actively characterized by multiple institutions [1,2,12,13]. While some basic properties such as tensile strength and ductility and microstructural data are available for multiple heats of the alloy, the knowledge base on other key properties such as weldability, corrosion resistance, creep and fracture behaviors is very limited. Since the alloy is developed for high temperature reactor applications, the high temperature creep and fracture resistance should be among the most essential properties. This study aimed at characterizing the high temperature fracture behavior of the latest heat of 14YWT alloy.

Fracture toughness tests at low temperatures (<200 °C) revealed that the 14YWT (SM6) had far superior fracture properties compared to its predecessor 12YWT alloy [11–13,19]: the 14YWT had a transition temperature T_0 of around −150 °C and the upper shelf fracture toughness of about 175 MPa $\sqrt{m}$. Considering that its tensile yield strength is very high: above 1.5 GPa at RT and higher at lower temperatures, such a high fracture toughness at or below RT is considered to be extraordinary. It has not been known, however, if such a high cracking resistance is retained at higher temperatures.

In this work, the static fracture toughness tests have been carried out in the temperature range of 22–700 °C using 12.5 mm diameter disk compact tension specimens. Fracture surfaces were examined in a scanning electron microscope. The experimental results were discussed focusing on the temperature dependences of fracture toughness and corresponding fracture surfaces. This study also intended to find the origin of poor high temperature fracture behavior in the NFA 14YWT and to provide feedbacks for process development.

2. Experimental

The 14YWT alloy examined in this work was the SM10 heat that was produced by mechanical-alloying a mixture of pre-alloyed powder with particle size ranging from 45 to 150 μm and 0.3% Y_2O_3 powder having a particle size ranging from 17 to 31 nm. The pre-alloyed steel powder was produced by Ar gas atomization by Special Metals Powder Division. The powder mixture was ball-milled in Zoz CMO1 attritor mil for 40 h in a static Ar environment. The mechanically-alloyed powder was filled into a mild steel can which was evacuated to a vacuum of ~1 Pa at 400 °C, sealed and hot-extruded at 850 °C [2]. This heat was annealed at 1000 °C for 1 h and hot-rolled at 850 °C to 40% reduction in thickness parallel to the extrusion direction. Since this test material is strengthened

* Corresponding author. Address: Oak Ridge National Laboratory, 1 Bethel Valley Rd., Oak Ridge, TN 37831, USA. Tel.: +1 865 576 7738.
E-mail address: byunts@ornl.gov (T.S. Byun).
[1] Visiting Scientists from Korea Institute of Materials Science & Korea Atomic Energy Research Institute, respectively.

0022-3115/$ - see front matter Published by Elsevier B.V.
doi:10.1016/j.jnucmat.2010.09.031

by both grain refinement and nanocluster dispersion, it has ultra high yield strengths: for example, 1600, 1230, and 550 MPa at RT, 500 °C, and 700 °C, respectively [20,21].

The specimen type used for the static fracture testing was a subsize disk compact tension (DCT) specimen with the nominal dimensions of 12.5 mm in diameter and 3 mm in thickness and with a 6.35 mm long wire-cut notch. All specimens had L–T orientation, in which the loading direction is in the extrusion direction and crack extension occurs perpendicularly. Precracking to produce sharp crack tip was carried out for each specimen under a nominal cyclic load of 400 ± 350 N at 30 Hz until the machined notch extended by 1.5–2 mm. Nominal crack length-to-specimen width ratio (a/W) was about 0.48 before fracture testing.

Static fracture toughness or fracture resistance (J–R) tests have been performed for the DCT specimens in a MTS servohydraulic testing machine equipped with a high vacuum, high temperature furnace. The J–R tests were conducted in stroke (displacement) control mode at a cross head speed of 0.005 mm/s with an unloading (by 20% of load)-reloading cycle at every 0.05 mm load-line displacement. The test and analysis followed the procedure described in the ASTM Standard E 1820-01 [22]. Each specimen was soaked at target temperature for about 10 min before testing and test temperature was controlled within ±1 °C. Also, nominal vacuum level was $\sim 10^{-6}$ torr during testing at high temperatures. The load versus load-line displacement curves with unloading–reloading cycles were recorded and used for analyses to obtain the interim fracture toughness (J_Q) data. Then, the fracture toughness data in the form of stress intensity factor, K_{JQ}, were obtained using the relationship:

$$K_{JQ} = \sqrt{(J_Q \cdot E)/(1 - \nu^2)} \quad (1)$$

where E is the Young's modulus at given temperature and ν the Poisson ratio (=0.28).

Fractography was also carried out in a scanning electron microscope (SEM) to compare fracture surface features. Images for the fracture surfaces were obtained at lower than 10 kV at various magnifications. This SEM examination aimed at elucidating the origin of low-ductility fracture behavior in conjunction with the fracture toughness data.

3. Results and discussion

3.1. Temperature dependence of fracture toughness

Fig. 1 compares the fracture toughness data (K_{JQ}) of 14YWT (SM10) with those of a HT-9 steel. The data for HT-9 steel (a 12Cr steel) were produced for the comparison purpose only. The fracture toughness values of 14YWT alloy at RT and 200 °C were 143 and 144 MPa $\sqrt{m}$ (J_Q = 90 and 95 kN/m), respectively. Above 200 °C the fracture toughness decreased to a significantly lower level of 52–82 MPa $\sqrt{m}$ (15–34 kN/m). Since the ductile-to-brittle transition of this alloy is below room temperature [12,13], the fracture toughness measured at 200 °C, 144 MPa $\sqrt{m}$, is believed to be the peak or upper shelf fracture toughness. Although the upper shelf toughness of the 14YWT alloy is much lower compared to the HT-9 steel, for which $K_{JQ} > 210$ MPa $\sqrt{m}$, the peak fracture toughness of 14YWT is believed to be acceptable considering its extraordinarily high strength in the temperature range ($\geqslant$1.5 GPa). Since the target application temperature for 14YWT alloy will be 500 °C or higher, however, the relatively low fracture toughness above 200 °C ($\leqslant$82 MPa $\sqrt{m}$) needs to be improved.

In addition to the low fracture toughness at elevated temperatures, another notable behavior found in the 14YWT alloy is its temperature dependence. The typical temperature dependence of fracture toughness for ferritic steels is that it increases up to a peak point within upper shelf region and then decreases gradually with increasing test temperature as seen in the HT-9 curve, Fig. 1. In the 14YWT alloy, however, the fracture toughness decreased rather abruptly to about a half of the peak toughness (in MPa $\sqrt{m}$ unit) between 200 and 300 °C and remained at the level in the range of 300–700 °C. In the traditional ferritic steels, the gradual decrease of fracture toughness with temperature after peaking can be explained by a combined effect of gradual change in plasticity and constraint around the crack tip and decreasing strength. Thus such a sudden drop of fracture toughness in the 14YWT alloy should be explained by a different cause such as a change in fracture mechanism in the 200–300 °C region.

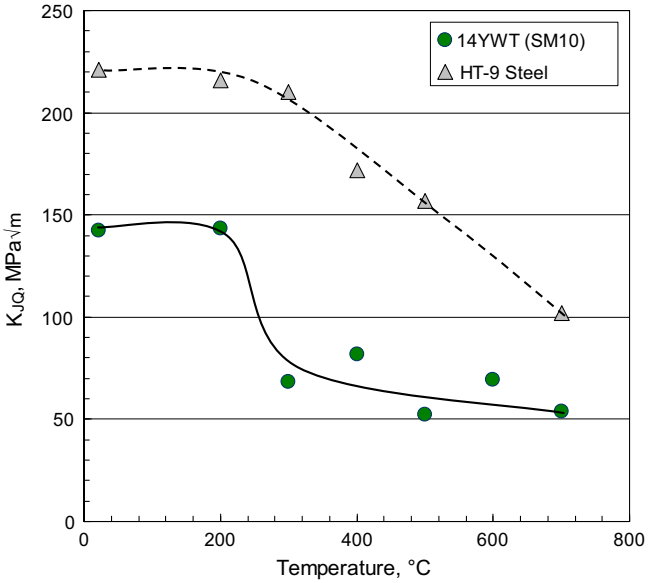

Fig. 1. Comparison of fracture toughnesses as a function of test temperature.

3.2. Temperature dependence of fracture surface

Fig. 2a–c compare the fracture surfaces in the same magnification (~2000X) after stable crack growth at representative temperatures: RT, 500 °C and 700 °C, respectively. The fracture surface from RT test comprises a mixture of numerous nanoscale dimples and cleavage facets. Most of these cleavage facets cover near-circular, isolated areas with diameters of one to several micrometers and are decorated with shear lips at their edges and often surrounded by small dimples. It should be recognized that the profile of the cleavages with shear lips and ductile dimples are quite shallow although those have surely involved significant local plasticity in formation. With these mixed features, therefore, the fracture at RT can be classified as a quasi-ductile fracture. Details in Fig. 2a can reveal more unique features of a high strength nanostructured alloy. Some small cleavage facets surrounded by shear lips are often not discernable from the nanoscale dimples. This may be because both the ductile dimple and the cleavage facet with shear lips would look alike if they were formed by either intergranular debonding or transgranular cleavage and were accompanied by significant plasticity surrounding the detached area. The second unique feature is the existence of the deep holes that are believed to originate from the gas pores survived the hot forming/sintering process. Along with the cleavage facets, these holes should act as crack initiation sites. Another noticeable feature might be the crevices or microcracks propagating to the surface normal direction. This feature is often observed in the low ductility materials with lamellar structures such as wrought molybdenum alloys [23,24]. This also indicates the existence of high internal stress at the lamellar boundaries.

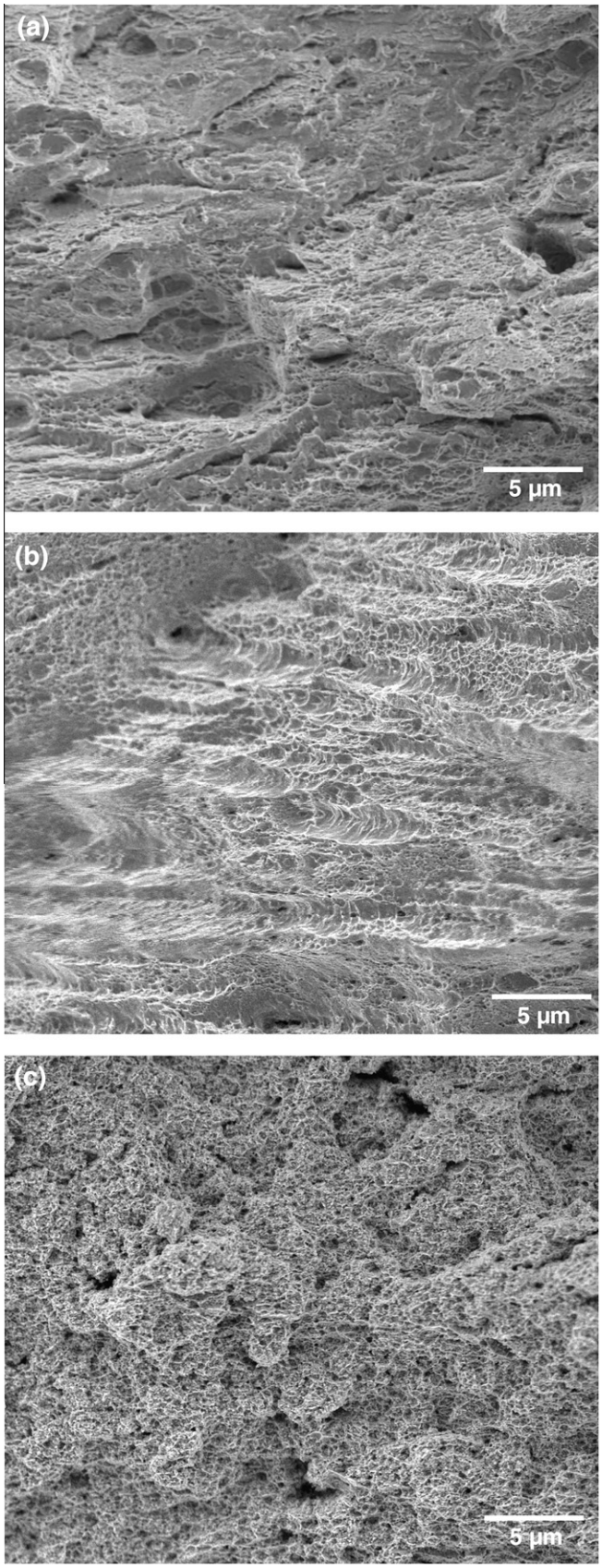

Fig. 2. Temperature dependence of fracture surface: the SEM images after fracture tests at: (a) RT, (b) 500 °C, and (c) 700 °C.

Fig. 2b formed at 500 °C displays well-developed dimple structure. However, the dimples are rather shallow, and again, their sizes are mostly in submicrometer range. Also, many of the dimples are preferably aligned along the crack propagation direction due to the influence of hot working process. The sizes of beehive-like dimples range from a few hundred nanometers to a few micrometers, but there are long, relatively flat areas enclosed by shear lips, in which very shallow dimples or shear lips are shown as substructures. It is believed that these areas are the surfaces produced by decohesion of multiple grains. The sizes of the substructures within these areas are similar to or larger than those of small dimples. The fracture surface formed at 500 °C appears to be a typical ductile fracture surface consisted primarily of dimples, but it actually is formed in a very fine scale by the decohesion of nanograins or their conglomerates. Fig. 2c obtained at 700 °C also displays very fine dimpled structure, in which the dimple sizes are about 1 μm or smaller. This image shows additional unique features such as the small holes or microcracks formed in the perpendicular direction to the plane and lifted-up surfaces including many dimples on them. Overall, the surface structure formed at 700 °C is considered less ductile than that formed at 500 °C.

3.3. Fracture toughness and mechanism

As discussed above, the change from quasi-ductile to ductile fracture surface with increasing temperature from RT to 500 °C may be an expected behavior. With increasing test temperature to 700 °C, however, the fracture surface changed to that of more brittle failure. Comparing the temperature dependences of fracture toughness and fracture surface, some questions arise about the reason for the less ductile fracture surface produced at a higher temperature of 700 °C and about the significant drop of fracture toughness from 143 MPa $\sqrt{m}$ at RT to 53 MPa $\sqrt{m}$ at 500 °C despite the fracture surface characteristics change from quasi-ductile to fully ductile.

The first question can be answered when the high magnification images in Fig. 3 are compared: the 500 °C image in Fig. 3a consists of shallow but ductile dimples with a lot of shear lips, while the 700 °C image in Fig. 3b reveals a dimpled structure with numerous particles comprising dimple walls and bottoms. In Fig. 3b the dimple boundaries are not as distinctive as in Fig. 3a and shear lips are less obvious. Considering their sizes ranging from tens of nanometers to a few hundred nanometers, the small particles are believed to be small grains, whose sizes are 136 ± 14 nm (95% confidence). These particles appear to be not much deformed individually. These features suggest that the 14YWT alloy in the form of aggregated nanograins becomes viscoplastic at 700 °C as the grain boundary slip becomes more eligible for plasticity under the high stress at crack tip. This picture also shows that dimples are much larger than grains and are formed by the boundary decohesion process most likely along aggregate boundaries. Such a mechanism of slip and decohesion at grain boundaries with little in-grain plasticity should result in a low fracture toughness.

Here, it is worth noting that the small cleavages found at RT specimen have not propagated through entire specimen but their growth has been stopped by formation of surrounding dimpled area, as seen in Fig. 2a. Fig. 3c shows a dimpled area formed at RT, where various fracture surface features such as holes, crevices, and shear lips are seen. Although these would not be always from highly ductile fracture, the low-energy grain boundary decohesion seen in Fig. 3b was not observed at RT.

The second question can be answered by a comparison of lower magnification images, Fig. 4a–c. Although the fracture surfaces seen in submicron scale are full of substructures such as dimples and/or cleavage facets, the low magnification images show much smoother surfaces except for some steps, longitudinal cracks, and lifted-up tongues. These smooth-looking mesoscale surfaces are different from the typical brittle cleavage facets and turned out

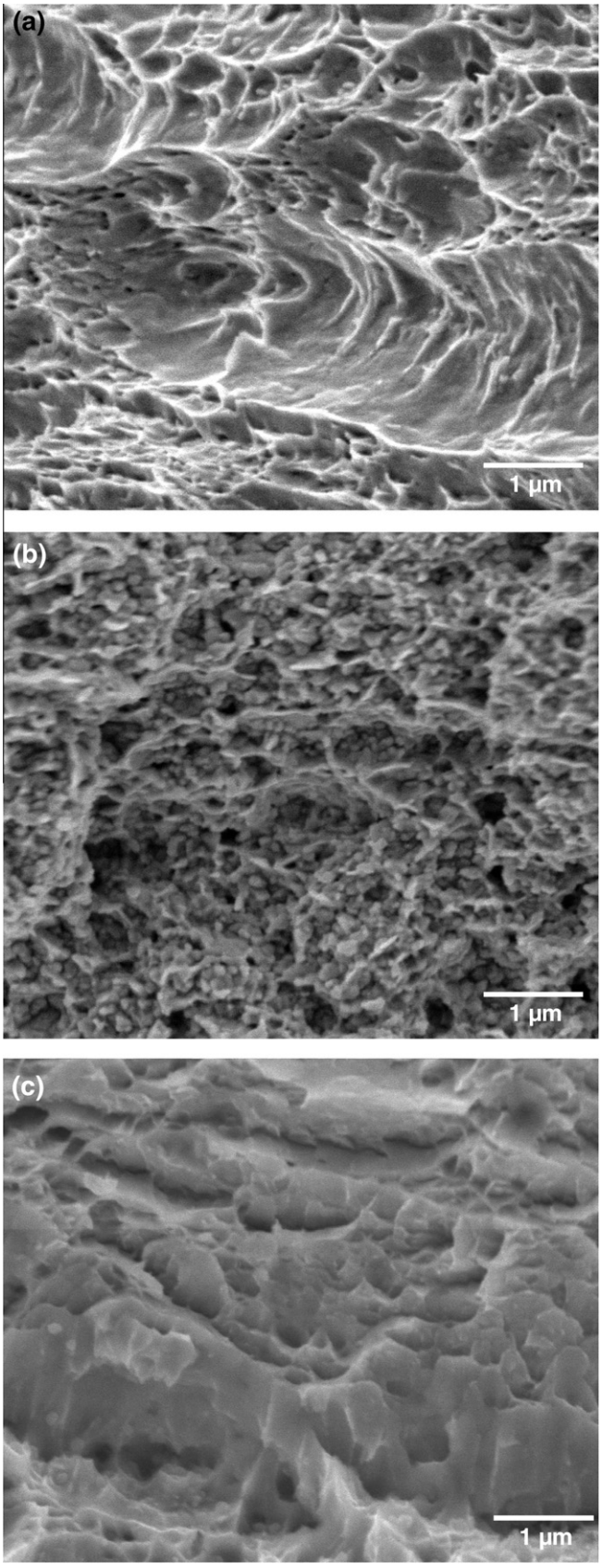

Fig. 3. Dimples observed at: (a) 500 °C, (b) 700 °C, and (c) RT.

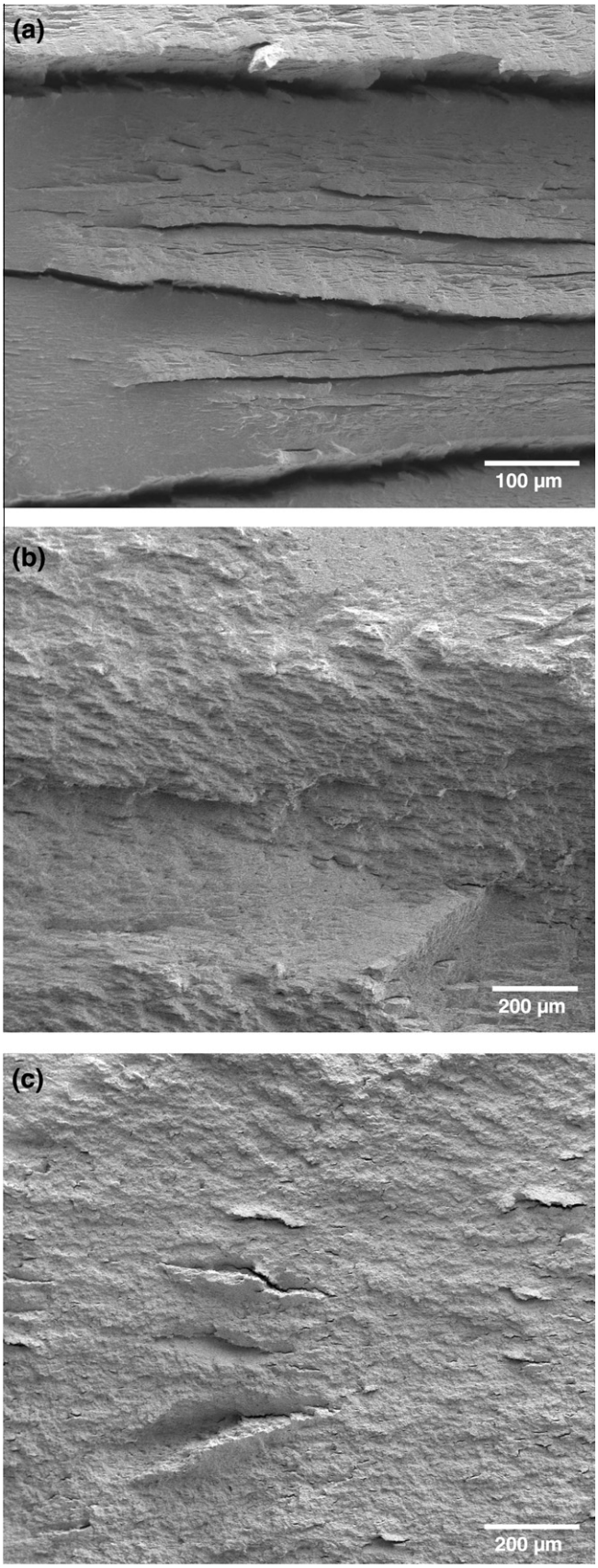

Fig. 4. Low magnification fracture surfaces obtained from: (a) RT, (b) 500 °C and (c) 700 °C tests. Crack propagation occurred from right to left.

to have very complex surfaces as seen in Figs. 2 and 3. Considering that the fracture surface with more ductile fracture features, Fig. 4b and c, resulted in lower fracture toughness, the fracture process occurring in a nanoscale is believed to have limited influence on fracture toughness. This may be because the fracture toughness is controlled by rather mesoscopic or macroscopic deformation and failure mechanisms and is dependent on the thickness of plastically deformed layer formed on the initiation of crack propagation. This indicates that the complex mesoscopic features like large steps and long longitudinal cracks in Fig. 4a have significantly contributed to the relatively high fracture toughness at RT and 200 °C. A higher toughness with less ductile features in nanoscale may be explained by a larger amount of absorbed energy during crack propagation: more energy should be absolved by formation of long cracks extended deeply into the specimen body and accompanying steps. With the smoother mesoscopic surface, Fig. 4b and c, however, the fracture process occurs in a shallow surface layer and thus the plasticity cannot penetrate deeply into material. Although the local plastic strain is very high at fracture surface with dimples, the high plasticity might penetrate into only a shallow layer with a thickness of probably a few times the dimple size. Combined with the lowered bonding strength at high temperature, such shallowness of plasticity zone should be the main reason for the low fracture toughness at high temperatures.

In observing the fracture surfaces we should recognize that the scale of microscopic fracture process in the 14YWT alloy is much smaller than those found in other ductile steels, in which dimple sizes are often a few to several micrometers [25,26]. Considering that the fracture toughness is directly proportional to the thickness and area of plastically deformed zone generated by the passage of crack tip, it is believed that the low fracture toughness behavior found with fully developed dimples can be improved by incorporating coarser obstacles that can deflect more cracks to form rougher surface. A higher strain hardening rate will be also effective since it can help to propagate plasticity into thicker layer. However, more fundamental remedy for increasing fracture toughness will be to increase the bonding strength between grains so that a higher local strain can be achieved and the surface plasticity can propagate into deeper material before fracture stress is reached at the surface.

Although it can be easily understood that the formation of crevice cracks and steps increases the total energy absorbed in fracture process, the underlining mechanism that eliminates the steps and crevice cracks above 200 °C is still not well understood and further study is needed. It is postulated here that the temperature dependence of dislocation mobility can explain the change of fracture surface and toughness between 200 °C and 300 °C. The disappearance of cleavage surfaces in Fig. 2b and c, which were formed at 500 °C and 700 °C, respectively, provides a basis for this postulation. Up to 200 °C the dislocation mobility is so low but the tensile fracture strength in the tensile loading direction is so high that the failure on the major fracture surface does not occur before the stress component in the transverse direction causes failure on the lamellar boundaries, Fig. 4a. These boundaries are formed by hot working in processing and are usually weaker than the boundaries with surface normal in the tensile direction (note that the specimens have L–T orientation). Above 200 °C, however, the dislocation mobility is high enough that the crack tip can advance by a fully plastic process that forms dimples. As discussed above, although the fracture process changes from mixed mode to fully plastic mode just above 200 °C, this plastic process cannot result in higher fracture toughness because of the shallow fracture process layer. Again, the fracture toughness remained low at >500 °C because of the enhanced slip and decohesion at grain boundaries.

4. Summary and conclusions

High temperature fracture behavior was investigated for the nanocluster strengthened 14YWT (SM10 heat) alloy. The fracture toughness of this alloy was above 140 MPa $\sqrt{m}$ at RT and 200 °C, however, it decreased to a low toughness range of 52–82 MPa $\sqrt{m}$ above 200 °C. It was believed that the low fracture toughness was caused by the formation of shallow plastic zone during crack propagation due to the unique nanostructure of the alloy, the existence of residual gas pores acting as crack initiation sites, and the low strain grain boundary decohesion at 700 °C due to weak bonding. It is suggested that the fracture toughness of the 14YWT alloy be improved by introducing a coarser microstructural feature that can deflect cracks and absorb more energy, reducing gas-trapped pores, and/or strengthening boundaries through changes in the mechanical-alloying and thermo-mechanical treatment conditions.

Acknowledgements

This research was sponsored by US Department of Energy, Office of Nuclear Energy under Contract DE-AC05-00OR22725 with UT-Battelle, LLC. It was also sponsored by the 2009 Scientist & Engineers Exchange Program supported by the Ministry of Knowledge Economy of the Republic of Korea. The authors would like to express special thanks to Drs. J.T. Busby and L. Tan for their technical reviews and thoughtful comments.

References

[1] M.J. Alinger, G.R. Odette, D.T. Hoelzer, Acta Mater. 57 (2009) 392–406.
[2] D.T. Hoelzer, J. Bentley, M.A. Sokolov, M.K. Miller, G.R. Odette, M.J. Alinger, J. Nucl. Mater. 367–370 (2007) 166–172.
[3] G.R. Odette, M.J. Alinger, B.D. Wirth, Annu. Rev. Mater. Res. 38 (2008) 471–503.
[4] A. Kimura, Mater. Trans. 46 (2005) 394–404.
[5] S. Ukai, M. Harada, H. Okada, M. Inoue, S. Nomura, S. Shikakura, K. Asabe, T. Nishida, M. Fujiwara, J. Nucl. Mater. 204 (1993) 65–71.
[6] S. Ukai, M. Fujiwara, J. Nucl. Mater. 307 (2001) 749–757.
[7] S. Ukai, T. Nishida, T. Okuda, T. Yoshitake, J. Nucl. Mater. 258 (1998) 1745–1749.
[8] K. Verhiest, A. Almazouzi, N. De Wispelaere, R. Petrov, S. Claessens, J. Nucl. Mater. 385 (2009) 308–311.
[9] O. Miao, G.R. Odette, T. Yamamoto, M. Alinger, D. Klingensmith, J. Nucl. Mater. 377 (2009) 59–64.
[10] M.K. Miller, K.F. Russell, D.T. Hoelzer, J. Nucl. Mater. 351 (2006) 261–268.
[11] M.K. Miller, D.T. Hoelzer, E.A. Kenik, K.F. Russell, Intermetallics 13 (2005) 387–392.
[12] D.A. McClintock, D.T. Hoelzer, M.A. Sokolov, R.K. Nanstad, J. Nucl. Mater. 386 (2009) 307–311.
[13] D.A. McClintock, M.A. Sokolov, D.T. Hoelzer, R.K. Nanstad, J. Nucl. Mater. 392 (2009) 353–359.
[14] S. Ukai, S. Ohtsuka, T. Kaito, H. Sakasegawa, N. Chikata, S. Hayashi, S. Ohnuki, Mater. Sci. Eng. A 510–511 (2009) 115–120.
[15] S. Oh, J.S. Lee, C. Jang, A. Kimura, J. Nucl. Mater. 386 (2009) 503–506.
[16] H.S. Cho, R. Kasada, A. Kimura, J. Nucl. Mater. 367 (2007) 239–243.
[17] H. Kishimoto, R. Kasada, O. Hashitomi, A. Kimura, J. Nucl. Mater. 386 (2009) 533–536.
[18] N. Akasaka, S. Yamashita, T. Yoshitake, S. Ukai, A. Kimura, J. Nucl. Mater. 329 (2004) 1053–1056.
[19] M.A. Sokolov, D.T. Hoelzer, R.E. Stoller, D.A. McClintock, J. Nucl. Mater. 367–370 (2007) 213–216.
[20] J.H. Kim, T.S. Byun, D.T. Hoelzer, Tensile fracture characteristics of nanostructured ferritic alloy 14YWT, J. Nucl. Mater., accepted for publication.
[21] T.S. Byun, D.T. Hoelzer, G.R. Romanoski, D.A. McClintock, Thermomechanical Behavior of Nanostructured ODS Alloys, in: ICFRM-14 Conference, 2009, Sapporo, Japan.
[22] ASTM Standard E 1820-01, Standard Test Method for Measurement of Fracture Toughness.
[23] B.V. Cockeram, E.K. Ohriner, T.S. Byun, M.K. Miller, L.L. Snead, J. Nucl. Mater. 382 (2008) 229–241.
[24] B.V. Cockeram, R.W. Smith, K.J. Leonard, T.S. Byun, L.L. Snead, J. Nucl. Mater. 382 (2008) 1–23.
[25] A. Das, S. Tarafder, Int. J. Plast. 25 (2009) 2222–2247.
[26] B. Strnadel, Z. Jonšta, Eng. Frac. Mech. 48 (1994) 863–871.